Evolution of Water Vapor Concentrations and Stratospheric Age of Air in Coupled Chemistry-Climate Model Simulations

JOHN AUSTIN, JOHN WILSON, AND FENG LI

NOAA/Geophysical Fluid Dynamics Laboratory, Princeton, New Jersey

HOLGER VÖMEL

CIRES, University of Colorado, Boulder, Colorado

(Manuscript received 27 October 2005, in final form 5 July 2006)

ABSTRACT

Stratospheric water vapor concentrations and age of air are investigated in an ensemble of coupled chemistry-climate model simulations covering the period from 1960 to 2005. Observed greenhouse gas concentrations, halogen concentrations, aerosol amounts, and sea surface temperatures are all specified in the model as time-varying fields. The results are compared with two experiments (time-slice runs) with constant forcings for the years 1960 and 2000, in which the sea surface temperatures are set to the same climatological values, aerosol concentrations are fixed at background levels, while greenhouse gas and halogen concentrations are set to the values for the relevant years.

The time-slice runs indicate an increase in stratospheric water vapor from 1960 to 2000 due primarily to methane oxidation. The age of air is found to be significantly less in the year 2000 run than the 1960 run. The transient runs from 1960 to 2005 indicate broadly similar results: an increase in water vapor and a decrease in age of air. However, the results do not change gradually. The age of air decreases significantly only after about 1975, corresponding to the period of ozone reduction. The age of air is related to tropical upwelling, which determines the transport of methane into the stratosphere. Oxidation of increased methane from enhanced tropical upwelling results in higher water vapor amounts. In the model simulations, the rate of increase of stratospheric water vapor during the period of enhanced upwelling is up to twice the long-term mean. The concentration of stratospheric water vapor also increases following volcanic eruptions during the simulations.

1. Introduction

Measurements over Boulder, Colorado, since 1980 showing large unexplained increases in stratospheric water vapor (Oltmans et al. 2000) have stimulated considerable interest in the scientific community. Evidence for these increases having taken place over much longer periods have also been found (Rosenlof et al. 2001) and have occurred despite falling tropical tropopause temperatures over the last few decades (Seidel et al. 2001). In contrast, recent Halogen Occultation Experiment (HALOE; Russell et al. 1993; Harries et al. 1996) and Boulder in situ data (Randel et al. 2004) indicate that water amounts have decreased since about 2000. It now appears that water vapor concentrations in the lower stratosphere are, as expected, driven by tropical tropopause temperatures (Fueglistaler and Haynes 2005) and so the question remains how, despite an overall reduction in tropical tropopause temperatures over the period from 1978 to 1997 (Seidel et al. 2001), stratospheric water vapor concentrations could have increased between 1980 and 2000.

One explanation for the water vapor increase was tentatively put forward by Joshi and Shine (2003) suggesting that volcanic eruptions could be responsible, by temporarily heating the lower stratosphere and raising the saturated vapor pressure of water. Their calculations did not include methane oxidation, which is an important process in the stratosphere and they did not estimate how long the enhanced water would remain. Such calculations ideally require comprehensive coupled chemistry-climate models. One such calcula-

Corresponding author address: Dr. John Austin, NOAA/Geophysical Fluid Dynamics Laboratory, Princeton, NJ 08542-0308.
E-mail: john.austin@noaa.gov

DOI: 10.1175/JAS3866.1

tion was supplied by Dameris et al. (2005) but their conclusion was that volcanic eruptions have only a short time scale and hence water vapor perturbations from volcanoes would be insufficient to explain the increases of the last 20 years despite some noteworthy eruptions. Other works (e.g., Hartmann et al. 2001; Holton and Gettelman 2001) have explored the details of the freeze-drying process, but it is not clear that changes in freeze drying can lead to substantial water vapor changes without corresponding temperature changes.

In this paper, we investigate the evolution of stratospheric water vapor concentrations over the period 1960–2005 in simulations of a coupled chemistry-climate model with observed forcings. A small ensemble of simulations is completed to reduce the statistical uncertainties of the results and decadal timescale variations are compared with observations. The simulations were not designed specifically to investigate water vapor, but since most of the established atmospheric processes and forcings are present in the climate model, the simulations can be used to demonstrate plausibility arguments for the long-term water vapor changes that were observed.

Among the many chemical tracers in the model, stratospheric age of air (Waugh and Hall 2002, and references therein) is simulated as a clock tracer and found to be a useful diagnostic to understand the model results. This tracer is an indication of the residence time in the stratosphere and enables us to explore from a different perspective some of the issues raised by Joshi and Shine (2003) regarding the duration of time over which tropical tropopause impacts remain in the stratosphere. The age of air tracer together with model methane results also allows one of the major water vapor source terms to be investigated. Hence, the model results are used to address the role of methane oxidation and variations in tropical tropopause conditions in influencing bulk stratospheric water vapor concentrations.

2. Description of the model

The new model Atmospheric Model with Transport and Chemistry (AMTRAC) is used. This is an extension of the Geophysical Fluid Dynamics Laboratory (GFDL) Atmospheric Model (AM2; Anderson et al. 2004) with an additional 24 levels and a coupled troposphere–stratosphere photochemistry scheme. The model has 48 layers (see Fig. 1; Table 1) and has a grid with resolution approximately 2° latitude by 2.5° longitude. The upper boundary is at 0.002 hPa, although the top few levels are well spread out in the vertical (Fig. 1).

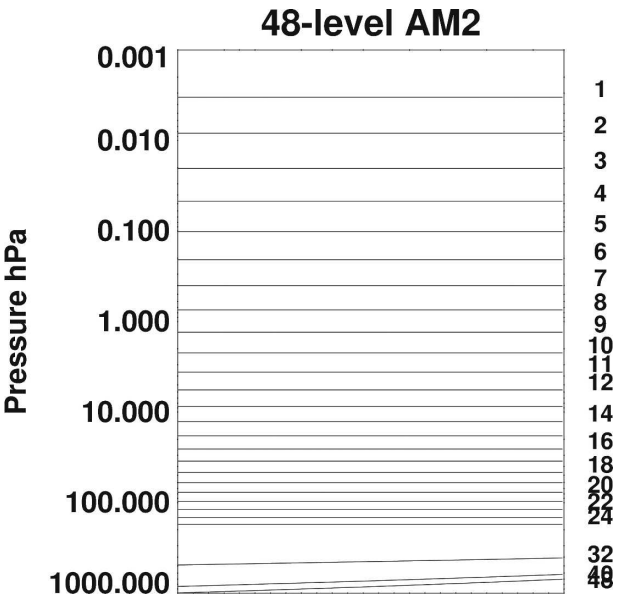

FIG. 1. Positions of the full levels in the model. The top 24 levels are indicated and have fixed pressure independent of surface pressure. The levels approach pure σ levels at the surface. Levels below level 24 are placed close together in log pressure coordinates and for clarity, only levels 28, 32, 40, and 48 are shown. The abscissa can be interpreted as any function giving rise to a surface pressure variation.

Below 600 hPa, the model levels are at similar pressures as in Anderson et al., but the resolution in the upper troposphere and stratosphere have been considerably increased. Above 300 hPa, the resolution has been increased by a factor of 2 or more.

All the physical and radiative processes are parameterized in the same way as Anderson et al. (2004), with the same parameters, except that the dynamical core and tracer transport are based on finite volume numerics (Lin 2004). In addition, the 48-level model used here has a nonorographic gravity wave forcing scheme due to Alexander and Dunkerton (1999) to represent the momentum source from breaking gravity waves. This version of the model does not exhibit a quasibiennial oscillation. Solar cycle variations are included in the radiative forcing (Lean et al. 1995, extended to 2005). For the model photochemical reaction rates, solar cycle effects were included as a linear function of the flux at the 10.7-cm wavelength. Data for the 10.7-cm radio flux were obtained from the National Geophysical Data Center and values measured at Ottawa were used.

The photochemical component of the model is an improved version of that used in the Met Office Unified Model with Eulerian Transport and Chemistry; UMETRAC; Austin and Butchart 2003, and references therein). All the key stratospheric ozone destruction

TABLE 1. Coefficients a_k and b_k for the calculation of the model pressure levels. The pressure p is given by $p = a_k + b_k p_s$, where p_s is surface pressure. Model layer 1 is centered between level 1 and level 2, etc.

k	a_k (Pa)	b_k (Pa)	p (Pa)
1	0.000	0.000 000	0.000
2	0.464	0.000 000	0.464
3	1.198	0.000 000	1.198
4	2.881	0.000 000	2.881
5	6.492	0.000 000	6.492
6	13.776	0.000 000	13.776
7	27.648	0.000 000	27.648
8	52.697	0.000 000	52.697
9	95.757	0.000 000	95.757
10	166.470	0.000 000	166.470
11	277.788	0.000 000	277.788
12	446.290	0.000 000	446.290
13	692.260	0.000 000	692.260
14	1039.440	0.000 000	1039.440
15	1514.442	0.000 000	1514.442
16	2145.846	0.000 000	2145.846
17	2963.012	0.000 000	2963.012
18	3994.736	0.000 000	3994.736
19	5267.824	0.000 000	5267.824
20	6805.733	0.000 000	6805.733
21	8627.367	0.000 000	8627.367
22	10 746.123	0.000 000	10 746.123
23	13 169.237	0.000 000	13 169.237
24	15 897.471	0.000 000	15 897.471
25	18 925.119	0.000 000	18 925.119
26	20 785.027	0.014 360	22 240.055
27	21 756.887	0.040 160	25 826.100
28	22 456.549	0.071 080	29 658.730
29	22 864.213	0.107 070	33 713.082
30	22 968.760	0.147 950	37 959.793
31	22 767.354	0.193 440	42 367.660
32	22 264.705	0.243 180	46 904.918
33	21 472.127	0.296 720	51 537.281
34	20 406.432	0.353 580	56 232.926
35	19 088.785	0.413 260	60 962.355
36	17 543.566	0.475 220	65 695.234
37	15 797.289	0.538 930	70 404.375
38	13 877.624	0.603 870	75 064.750
39	11 812.548	0.669 560	79 655.719
40	9865.883	0.728 520	83 683.172
41	8073.972	0.780 800	87 188.531
42	6458.083	0.826 600	90 213.328
43	5027.989	0.866 210	92 796.719
44	3784.610	0.900 040	94 981.164
45	2722.009	0.928 540	96 806.320
46	1828.974	0.952 210	98 311.656
47	1090.240	0.971 630	99 540.648
48	487.457	0.987 350	100 530.695
49	0.000	1.000 000	101 325.000

cycles (O_x, HO_x, NO_x, ClO_x, and BrO_x) are included explicitly as well as a simplified heterogeneous chemistry scheme of nitric acid trihydrate (NAT) or ice using the detailed parameterizations of Sander et al. (2003). In the troposphere, the chemistry is represented by methane oxidation processes and appropriate HO_x and NO_x reactions. An improvement since the Austin and Butchart (2003) work is the incorporation of additional chemistry for the computation of NO_y, which in UMETRAC was parameterized. Another innovation is the inclusion of mean age of air as a clock tracer. This variable is used in conjunction with chlorofluorocarbon (CFC) and halon photolysis rates inferred from measurements to compute the concentrations of Cl_y and Br_y. Reaction rates are taken from Sander et al. (2003).

Sedimentation of ice particles occurs in the cloud physics module of the climate model. Sedimentation of NAT particles occurs separately in the photochemistry scheme. Water vapor tendencies are computed in the photochemistry scheme and passed to the climate model. In particular, methane oxidation chemistry is computed explicitly, which leads to model water vapor increases over time. The chemistry is coupled to the climate via the ozone and water vapor amounts. Three-dimensional concentrations are used in the model radiation scheme, which is called every 3 h.

The model is forced with observed sea surface temperatures and sea ice amounts used in simulations of the climate model runs of Anderson et al. (2004). The long-lived greenhouse gases (GHGs) CO_2, CH_4, N_2O, and CFCs are specified from observations. For the radiation module their concentrations are taken to be uniformly mixed throughout the atmosphere. For the photochemical module, CH_4 and N_2O are relaxed to observed values in the troposphere (defined as where the age of air is less than 0.1 yr), and are computed explicitly in the stratosphere. Volcanic aerosol extinctions used in the radiation model are calculated using the method of Sato et al. (1993) for all model wavebands (Stenchikov et al. 1998). Near-IR extinctions are converted to surface area densities for the computation of the heterogeneous reaction rates using the parameterization of Thomason and Poole (1997). Figure 2 shows the tropospheric CH_4 and lower-stratospheric aerosol surface area densities used in the simulations. The major volcanic eruptions Agung, El Chichón, and Mt. Pinatubo are indicated in the figure by the rapid rise in values in 1963, 1982, and 1991.

3. Model simulations

The simulations completed are given in Table 2. A 30-yr time-slice experiment (SL1960) was first completed with 1960 concentrations of the GHGs and CFCs, and background aerosol concentrations. The solar forcing was set to a constant, midcycle value. Initial

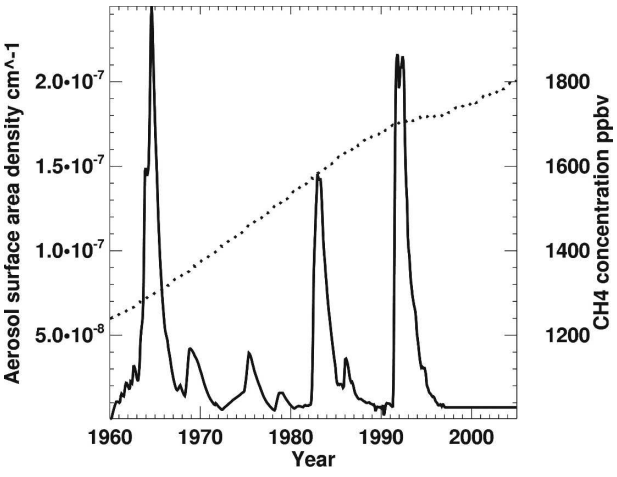

FIG. 2. Model forcing of CH_4 amounts (dotted line, right ordinate) and aerosol surface area density (solid line, left ordinate) as a function of year. The CH_4 mixing ratios (ppbv) are for the tropical lower troposphere. The aerosol data are for the equator at 60 hPa. The volcanic eruptions of Agung (1963), El Chichón (1982), and Mt. Pinatubo (1991) are indicated by the large increase in aerosol values.

conditions for this run were taken from previous model simulations except for water vapor, which was taken from current atmosphere observations. A 30-yr time-slice experiment for 2000 forcings (SL2000) was also completed using the same initial conditions. Both time-slice experiments used the same sea surface temperatures and sea ice (collectively referred to as SSTs) appropriate to the 1960–2000 period, so that differences between the two experiments could be attributed to GHG and CFC concentrations, as far as is possible in a climate model environment.

Three transient simulations for the period from 1960 to 2005 were initialized from years 10, 20 and 30 of the 1960 time-slice simulation (TRANSA, TRANSB, and TRANSC). Observed forcings were specified as functions of time for SSTs, the concentrations of GHGs and CFCs, aerosol extinction, and solar forcings. The model results for temperature, ozone, and other constituents have been compared briefly with observations in several publications (Austin and Wilson 2006; Eyring et al. 2006). Comparisons specifically relevant to water vapor are included in section 6.

4. Model results: Water vapor and methane

a. Water vapor

Figure 3 shows the zonal average concentration of water vapor in the model simulations at representative latitudes and pressures. Concentrations have large variations on all temporal scales, particularly in the lower stratosphere in the Antarctic. This is due in part to low temperatures during winter and spring and subsequent ice particle sedimentation. Typical annual ranges in the concentrations are given by the bars in the figure. Over the Antarctic, concentrations are much lower during winter than over the Arctic because much more sedimentation occurs. The concentrations for run SL2000 are generally higher than for SL1960 due to increased methane oxidation (section 4b). The upper-right panel of Fig. 3 shows the water vapor amount near the hygropause, where fluctuations are primarily due to changes in tropical tropopause temperature. In the Tropics (right panels) differences between the experiments are small at the hygropause and are dominated by interannual variability. In the tropical upper stratosphere, the 1960 time-slice results are significantly lower than in the other two experiments, due to differences in methane, noted earlier. Figure 3 illustrates the very large degree of variability even in the monthly averages, which has a bearing on comparisons with observations (section 6).

TABLE 2. Brief description of model simulations.

Expt	Description	Duration
SL1960	Time-slice 1960 conditions	30 yr
SL2000	Time-slice 2000 conditions	30 yr
TRANSA	Transient 1960–2005 Initialized year 10 of SL1960	45 yr
TRANSB	Transient 1960–2005 Initialized year 20 of SL1960	45 yr
TRANSC	Transient 1960–2005 Initialized year 30 of SL1960	45 yr

The longer-term variations in model water vapor are also displayed in Fig. 4, in which a 1-yr running mean has been calculated from the data in each experiment. To improve the signal further, the results were averaged over the indicated latitude bands. Each of the transient model runs has the same temporal behavior and, moreover, the model changes occur in steplike fashion rather than continuously. The temporal behavior of the model results is similar at all locations sufficiently far from the hygropause. The water vapor evolution is also qualitatively similar in the lower stratosphere where polar stratospheric cloud formation led to some sedimentation for a short period in the winter, especially over the Antarctic. In the Antarctic upper stratosphere (1.3 hPa), the annual average water vapor amount increased from 4.25 ± 0.03 (1σ) to 4.75 ± 0.03 for the period 1981 to 1995, an increase of 11.7 ± 1.0% in 14 yr. In the lower stratosphere, water vapor trends

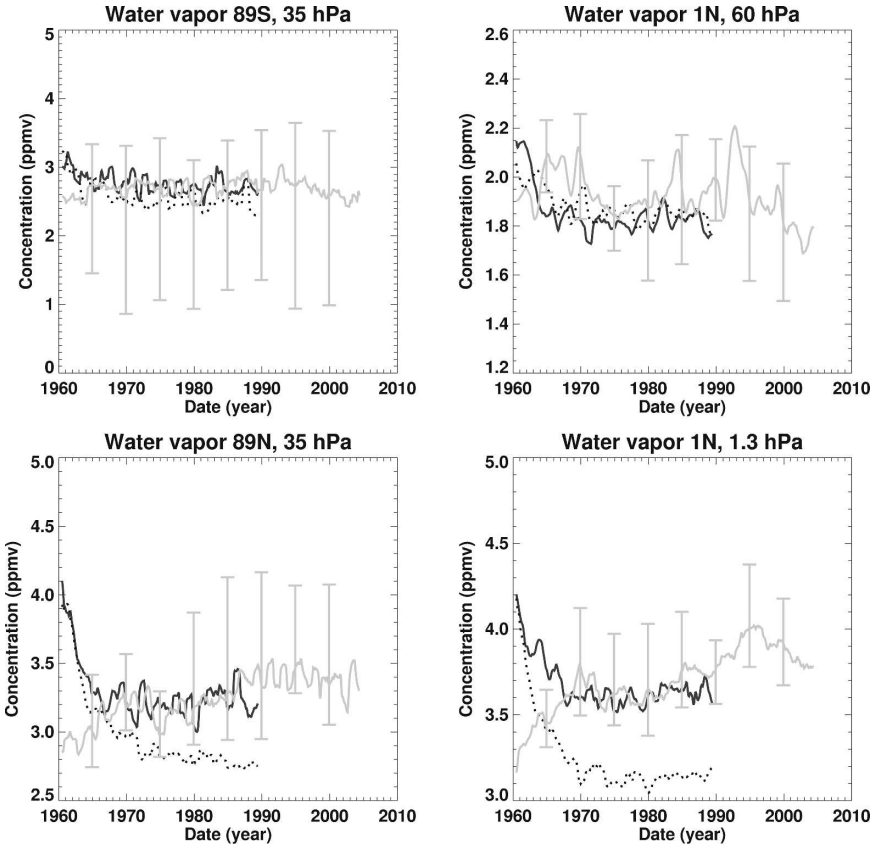

FIG. 3. Monthly and zonally averaged water vapor amounts at specified locations for runs SL1960 (dotted black), SL2000 (solid black), and TRANSA (solid gray). The bars denote the annual range of simulated values for run TRANSA. Note the different axis range in each panel.

were much smaller than in the upper stratosphere. Near the hygropause, the model water vapor concentrations are strongly affected by the tropical tropopause temperature.

b. Methane oxidation

It is recognized that methane oxidation is an important source of stratospheric water (Jones and Pyle 1984; Remsberg et al. 1984; Le Texier et al. 1988). This issue was investigated by exploring the total hydrogen in the model, which is conserved under mixing and transport. The quantity is given by $\mathcal{H} = H_2O + 2 \times CH_4 + H_2CO + H_2$ (plus additional radicals). Le Texier et al. (1988) provide a comprehensive analysis of methane oxidation and the number of water vapor molecules produced per methane molecule oxidized, here denoted by α. Conservation of $\mathcal{H}$ implies that α may differ from 2.0. Over long time scales in the absence of nonconservative processes $\mathcal{H}$ should then be uniform. An approximation of $\mathcal{H}$ by neglecting the last two terms has indeed been shown to be uniform in the stratosphere (e.g., Jones and Pyle 1984; Remsberg et al. 1984; Randel et al. 2004). However, this is not a particularly demanding test of conservation. Figure 5 shows model results from run TRANSA for January and July 2000 of the water vapor and $\mathcal{H}' = \mathcal{H}$, but with the last two terms approximated by a constant 0.5 ppmv. The contour interval of $\mathcal{H}'$ is one-tenth the contour interval for H_2O, indicating that in the absence of nonconservative processes, $\mathcal{H}'$ is uniform in the model to a much higher precision than can be measured. In the stratosphere there is some structure in the fields due to the approximation of the last two terms. Nonconservative processes, condensation, and evaporation occur in the troposphere and in the winter Antarctic lower stratosphere, as can be seen in the figure panels for July. Similar results occur for other years examined. This confirms that to a precision of about 0.05 ppmv, CH_4 oxidation can be taken as the major source term for water vapor.

Over the multidecadal period 1960–2005, the net wa-

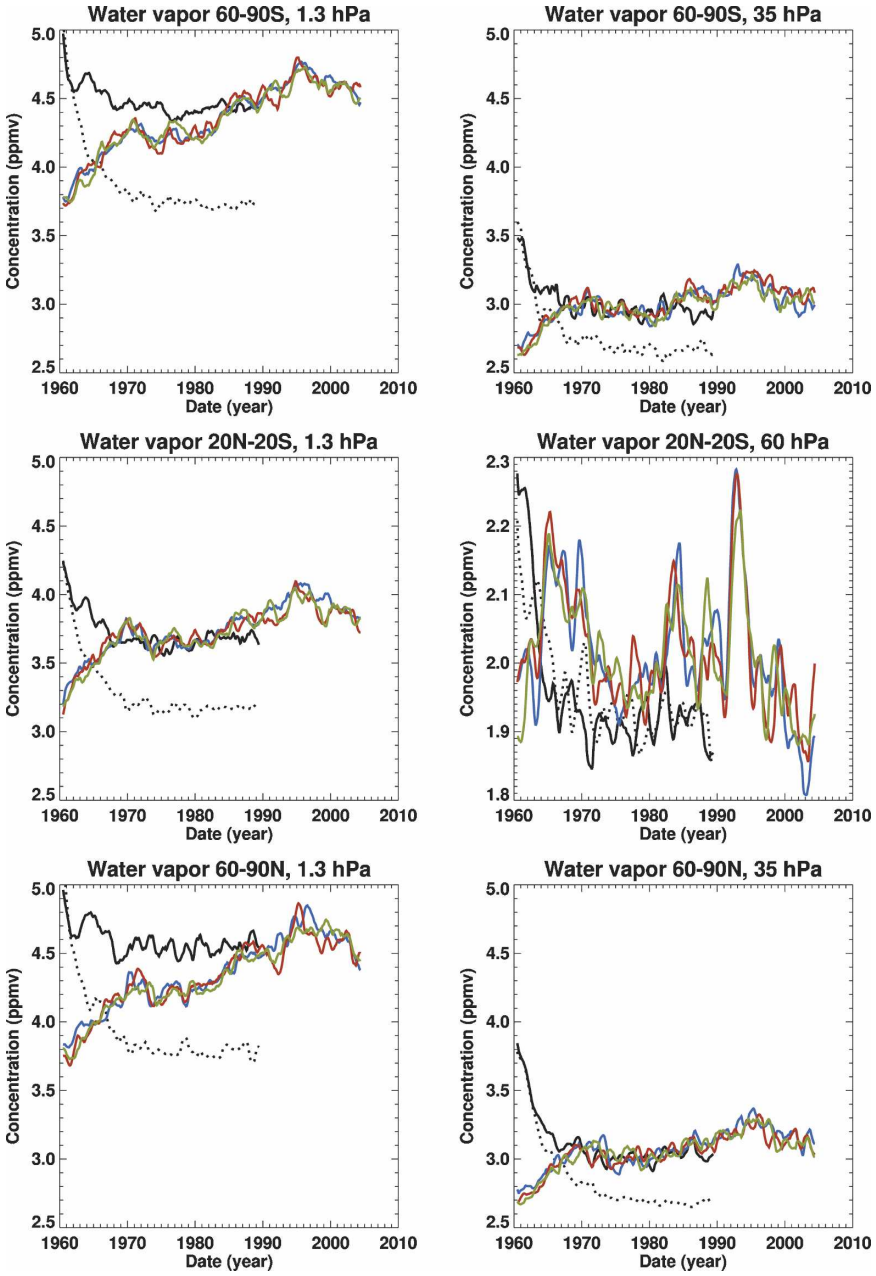

FIG. 4. Monthly and regionally averaged water vapor amounts at specified pressures for the model simulations. Solid black line is run SL2000, dotted black line is run SL1960, blue line is TRANSA, red line is TRANSB, green line is TRANSC. Each panel has the same axis range, except for the middle right panel.

ter vapor change in the bulk of the stratosphere for the transient runs was very similar to that obtained in the time-slice runs. In particular, in the upper stratosphere over the Antarctic, the difference in water vapor between the two time-slice runs was about 0.75 ppmv (Fig. 4), compared with the surface methane change of 0.51 ppmv. As the constituent concentration equation is linear in concentration, these values can be rescaled for the period 1981 to 1995. During this period, the tropospheric CH_4 concentration increased by 0.16 ppmv and hence the stratospheric water vapor would have been expected to have increased by 0.24 ppmv (6%) in the Antarctic upper stratosphere. During this period, the model water vapor increased by 12% (Fig. 4), about a factor of 2 larger than expected on the basis of the increase in tropospheric methane concentrations.

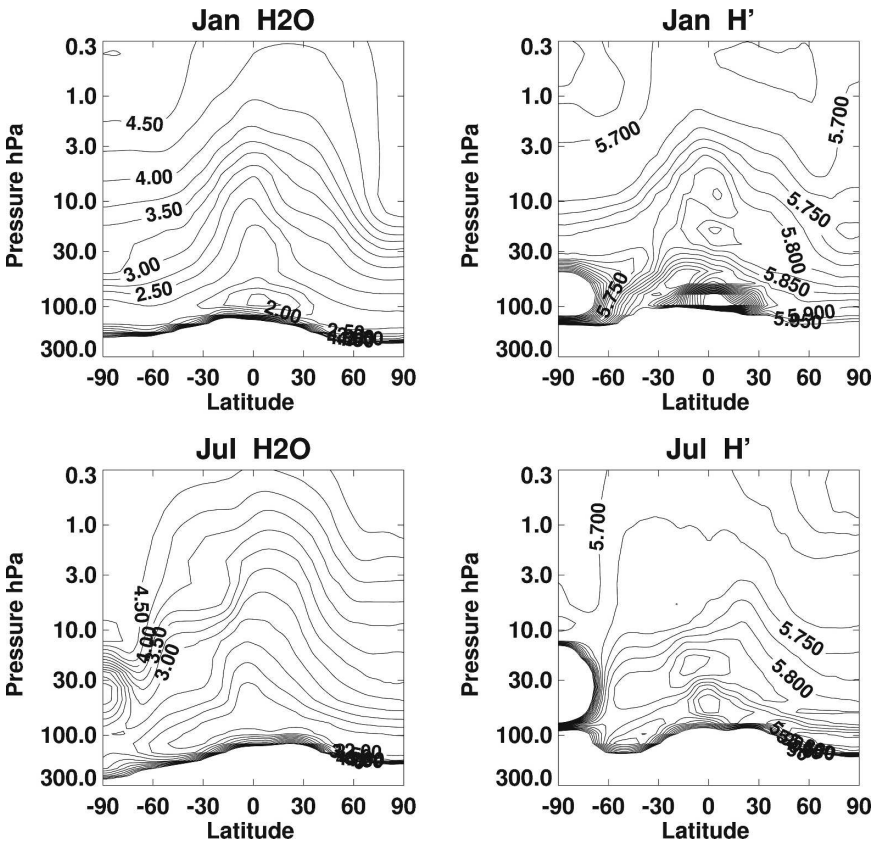

FIG. 5. Ensemble mean concentrations of water vapor and approximate $\mathcal{H}'$ for January and July 2000. The contour interval is 0.25 ppmv for H_2O and 0.025 for total H_2; H_2O is plotted in the range 0 to 5 ppmv, $\mathcal{H}'$ is plotted only in the range 5.5 to 6.0 ppmv.

c. The water vapor budget

The stratospheric water vapor amount at a given position and time is equal to the entry concentration plus an amount from methane oxidation. The entry into the stratosphere would have occurred at an earlier time, depending on air parcel position. Also, the amount of methane oxidation depends on the time since the air parcel resided in the troposphere. On the basis of Fig. 5, we can take to a very good approximation the factor of 2 for water vapor molecule production from methane oxidation. Thus, to a first approximation

$$H_2O(\theta, p, t) = A + B, \tag{1}$$

where $A = H_2O|_e(t - \tau)$ and $B = 2 \times [CH_4|_0(t - \tau) - CH_4(\theta, p, t)]$, θ is latitude, p pressure, and t time, $\tau = \tau(\theta, p, t)$ is the mean stratospheric age of air for the location, A is the water vapor entry volume mixing ratio, and B is the amount of H_2O produced from methane oxidation. In this approximation, it is assumed that the water vapor at stratospheric entry is approximately the same for all air parcels and that the temporal variations (through the age of air) are more important than the spatial variations. The age of stratospheric air appears in both A and B terms, and thus the results are sensitive to the mean age. This is explored further in section 5.

Successive water vapor approximations are shown in Fig. 6 compared with the actual model simulated water vapor (solid black line). Results are shown for the ensemble mean, but each of the individual experiments showed very similar results. Values are shown relative to 1980 and the CH_4 oxidation term averaged for the period 1965–2005 has been removed from the results to emphasize the differences. Water vapor amounts at stratospheric entry, term A, were determined by subtracting the small methane oxidation term, term B, from the model H_2O for the tropical region at 60 hPa.

The red lines (term B) have mostly positive tendencies during the period from about 1980 to about 1997, implying that methane oxidation is higher than would be calculated with fixed mean transport. The blue lines [right-hand side of Eq. (1)] agree well with the solid black lines, confirming the first-order accuracy of Eq.

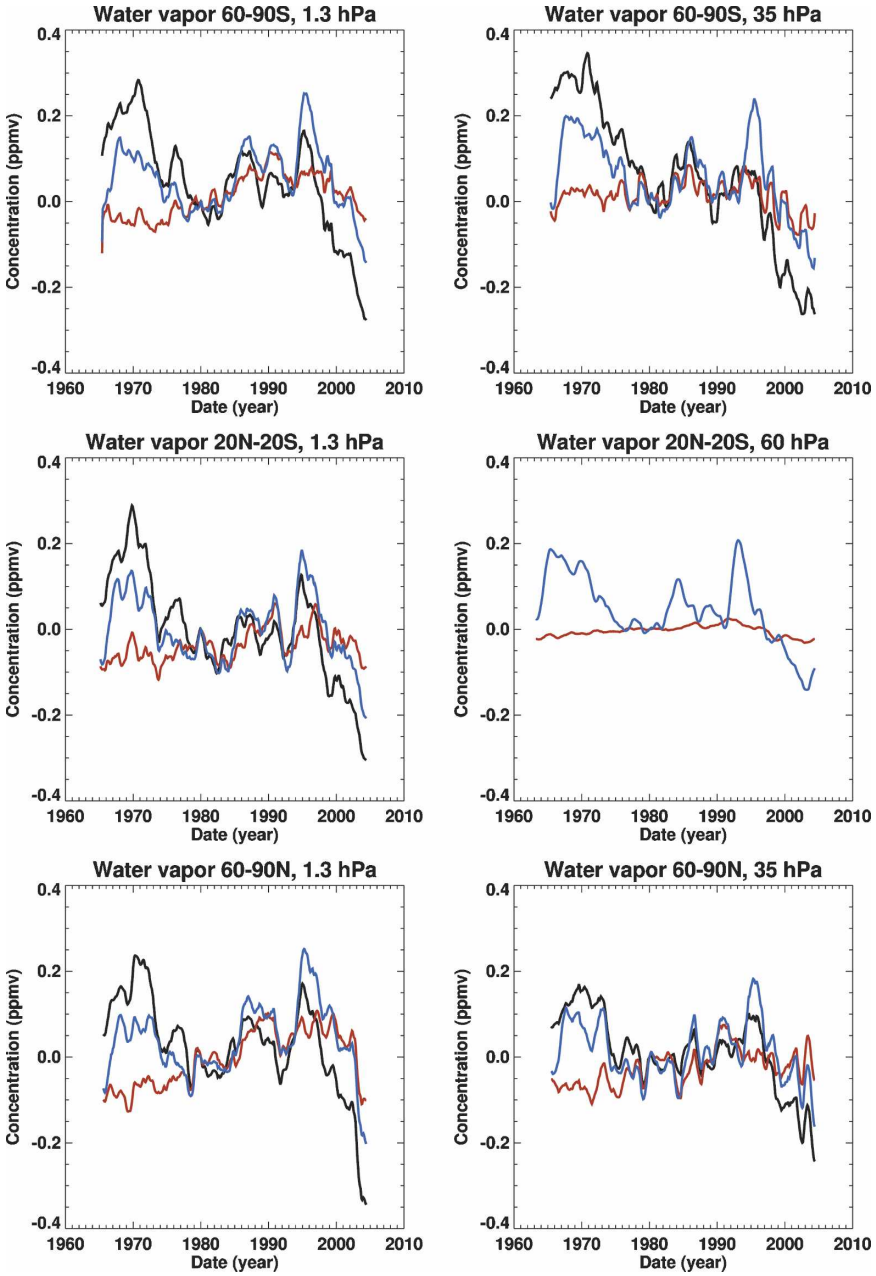

FIG. 6. Successive approximations to the water vapor concentration anomalies, averaged for all three ensemble members, at selected levels corresponding to Fig. 3. Results are expressed relative to 1980 concentrations after removing the mean CH_4, oxidation term *B*. Solid black lines is model water vapor. Red lines are CH_4 oxidation (term *B*) in Eq. (1). Blue lines are water vapor stratospheric entry term (term *A*) plus CH_4 oxidation term (term *B*).

(1) and indicating the importance of the stratospheric water vapor entry term. As noted in section 4a the three major volcanoes during the simulations triggered a temperature and water vapor (Figs. 3 and 4) response in the Tropics at 60 hPa. This effect occurred throughout the model domain, as indicated by the difference between the red and blue lines in Fig. 6. For example, in the upper stratosphere, differences between the red and blue curves became largest during the mid-1960s, the mid-1980s, and the mid-1990s, when the volcanic signals (Fig. 2) had propagated to the upper stratosphere. After the mid-1990s, the water vapor concentration in the model decreased significantly, which was well reproduced by the blue line, but less so by the red curve.

During this period, the individual curves in Fig. 6 indicate that the methane oxidation change and stratospheric entry amount have had a comparable impact on the decrease in model water vapor since 1995.

d. Summary

To summarize the results, the increase of water vapor in the model between the early 1980s and the mid-1990s was due to enhanced methane oxidation combined with an increase of water vapor concentration at stratospheric entry. A similar period of enhanced stratospheric water vapor occurred in the model in 1970 was caused primarily by enhanced stratospheric entry. While some of the large increases in stratospheric water entry can be identified as due to volcanic eruptions, tropospheric changes will likely have additionally contributed.

5. Model results: Age of air and the relationship with transport

In the previous section the source terms of stratospheric water were explored using a simplified expression [Eq. (1)]. Evaluation of the individual terms was shown in Fig. 6 to provide insight into periods when the water vapor entry term (term A) was significant and when variations in the CH_4 oxidation term (term B) was important. Both terms involve the stratospheric age of air implicitly in their description. Using results from the simulations presented here, Austin and Li (2006) have also shown that age of air is related to the mass upwelling. In this section, we present the related diagnostics of age of air and tropical upwelling to provide insight into the modeled CH_4 transport rate.

a. Model simulated mean age of air

As shown by previous authors, the mean age of air increases above the tropopause and peaks at about 6 yr (Boering et al. 1996; Andrews et al. 2001; Waugh and Hall 2002). More recent work gives derived age of air values, which are up to one year younger (Schoeberl et al. 2005). However, in common with most models (Park et al. 1999; Hall et al. 1999), AMTRAC underpredicts age of air giving peak values in the upper stratosphere of less than 4.5 yr for the current atmosphere. Figure 7 shows the results obtained in the model simulations, averaged over the same domains as the water vapor results of Fig. 4. Age in the 1960 time-slice run was about 15% higher than in the 2000 run. For the transient runs a consistent pattern occurred at all locations examined: after a few years the age remained approximately constant until the late 1970s and then decreased significantly by about 20% depending on location. In the tropical hygropause region, age of air decreased from about 0.95 yr to about 0.7 yr (30%) from 1978 to 1998. Over the full 45-yr transient simulation, changes in the age of air, as in the case of water vapor change, are similar to the differences between the two time-slice experiments.

b. The derived lower-stratospheric upward mass flux

Calculations of the meridional streamfunction from the residual circulation have been shown by Austin et al. (2003) for a range of models (see their Fig. 7). To compute the upward mass flux, the streamfunction was first calculated directly from the AMTRAC meteorological fields using daily data. The streamfunction peaks in the northern subtropics and moves slightly poleward with northern summer. The streamfunction also has a minimum in the southern subtropics, which moves slightly poleward with southern summer. This implies upward mass flux between the two subtropical latitudes, as discussed by Butchart and Scaife (2001). Those authors refer to the region of upward mass flux as contained by the turnaround latitudes and are shown in Fig. 8 (left panel for AMTRAC ensemble mean. Similar results were obtained for each run of the ensemble. The difference in streamfunction between the turnaround latitudes gives the upward mass flux (Fig. 8, right panel). The AMTRAC model results compare very well with the results obtained by Butchart and Scaife (2001) in showing very similar turnaround latitudes, but the overall increase in annual mean upwelling averaged over all three experiments of 9.2×10^8 kg $s^{-1} \pm 1.0(1\sigma)$ in 45 yr is almost twice the mean model value of Butchart et al. (2006) for assorted periods. AMTRAC also has higher absolute mass flux values. Figure 1 of Butchart and Scaife (2001) show the results from an 11-yr running mean and this smoothing is also used in Fig. 8. The smoothing has the advantage of removing some model noise, but it is likely that an important part of the signal has been lost in the process.

Figure 9 shows the upward mass fluxes with a 1-yr running average calculated from the results of all three ensemble members. All the ensemble members have very similar results suggesting that most of the variations are driven by external processes, rather than by internal model variability. For the period 1960 to the late 1970s there was no discernible systematic change in the mass flux. Similarly, after 2000 the results, if anything, show a slight decline. For the period from 1960 to 1974 the ensemble mean trend was $-0.3 \pm 1.3\%$ decade^{-1}, compared with $4.2 \pm 0.65\%$ decade^{-1} for the period 1975 to 1999. Qualitatively, the results show op-

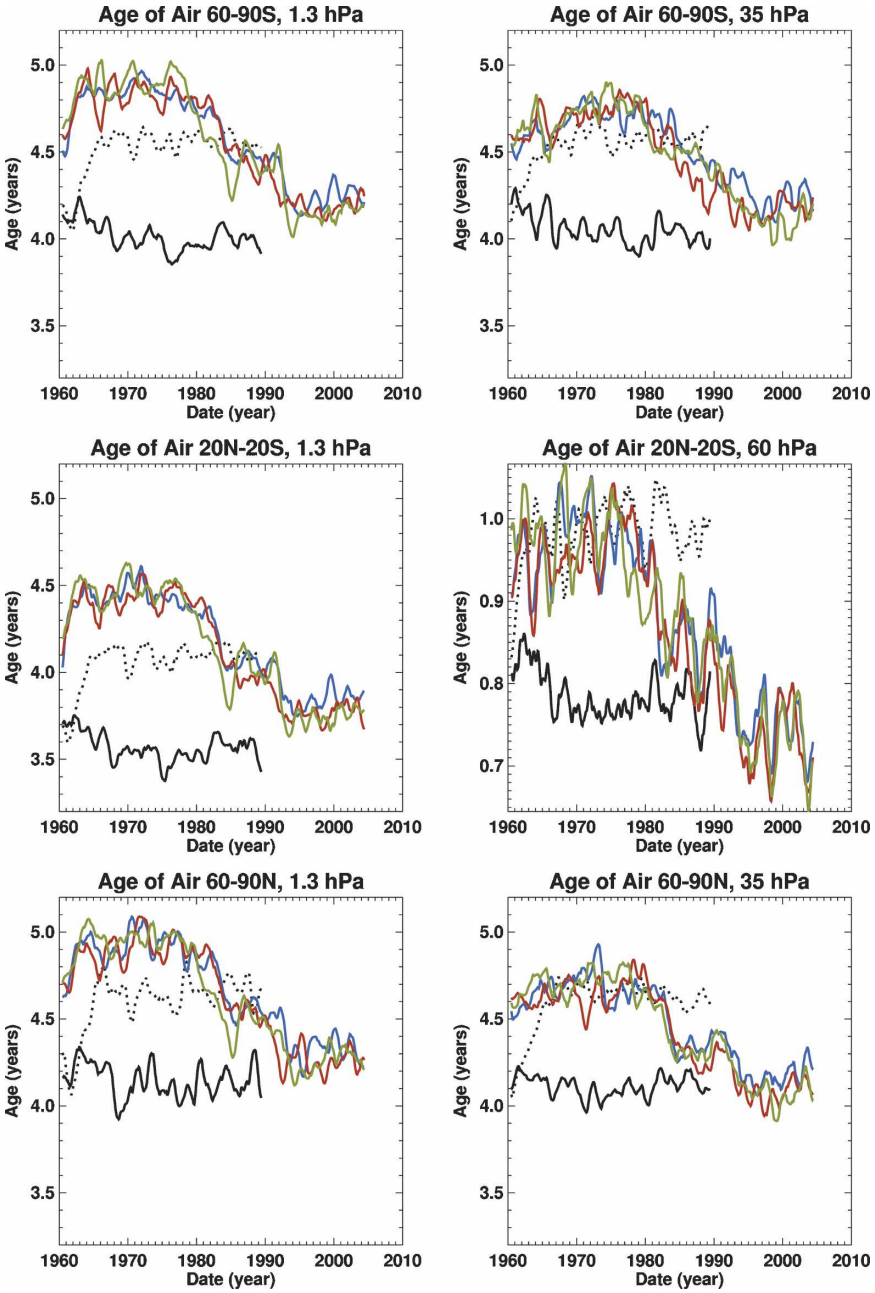

FIG. 7. Monthly and regionally averaged age of air at specified pressures for the model simulations. Solid black line is run SL2000, dotted black line is run SL1960, blue line is TRANSA, red line is TRANSB, green line is TRANSC. The values plotted are 12-month running means.

posite trends to those seen in the age of air (Fig. 7), except for the first 2 yr of the model simulations when the results were influenced by the initial conditions.

In summary, the results are consistent in showing increased tropical upwelling and equivalently, reduced stratospheric age of air between the early 1980s and the late 1990s. The effect of this would have been to transport more methane into the stratosphere for subsequent oxidation to water vapor, as shown in Fig. 6 (section 4c).

6. Comparison with observations

As shown in the previous section, an analysis of the model results has demonstrated the reasons for the simulated long-term water vapor increases. In this sec-

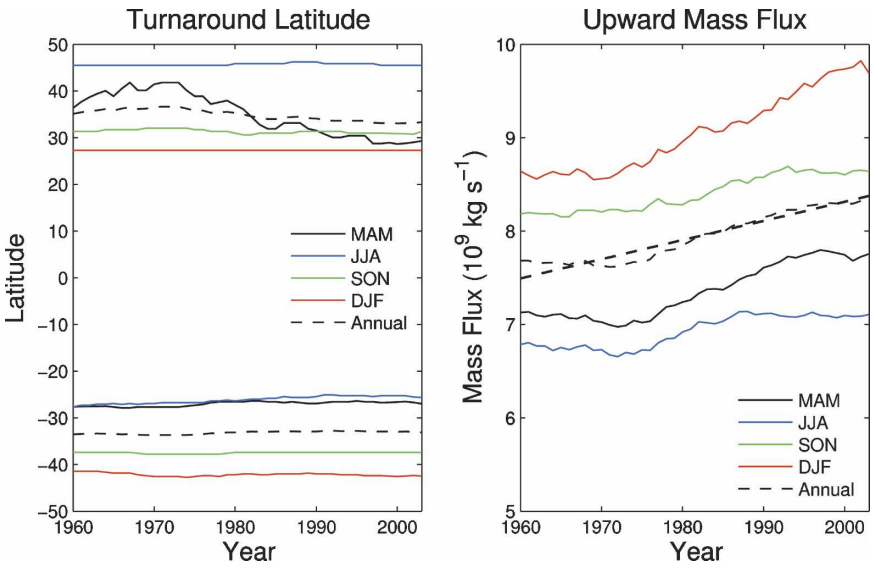

FIG. 8. The turnaround latitude and upward mass flux at 77 hPa for the four seasons and the annual mean, averaged for the three ensemble members. Data for an 11-yr running average are plotted. The thick black line in the right panel is the linear regression line through the annual data.

tion, the extent to which these processes may have operated in the atmosphere is investigated using comparisons with observations.

The change in circulation in the model was found to be important in simulating an increase in water vapor concentrations, but no direct measurements of stratospheric age exist. Instead we have investigated the tropical upward mass flux that has been shown by Butchart and Scaife (2001) to increase in climate model simulations. Calculations of the tropical upwelling using the 40-yr European Centre for Medium-Range Weather Forecasts Re-Analysis data (ERA-40 data, available from the Web site http://www.ecmwf.int) were inconclusive. Systematic variations in this quantity were difficult to discern, probably because of the highly derived nature of the diagnostic, the change in observation mix during the period (Rood 2005), and possibly spurious meridional circulations induced by the assimilation process. Hence, we focus on the tropical temperatures and the water vapor values themselves.

a. Lower-stratospheric temperatures

Figure 10 shows the ensemble mean temperature anomalies averaged over the Tropics near the hygropause (left panel) and the globally averaged temperature weighted in the vertical by the Microwave Sounding Unit Channel 4 (MSU4) weighting function (Christy et al. 2000). The anomalies in both panels are relative to the respective mean for the period from 1970 to 1999. The tropical temperatures are annually smoothed but still show substantial variations. The model simulated an overall cooling of about 2 K during the 40 yr, similar to that observed. Volcanic impacts are apparent in both model and observations following the eruptions of Agung (1963), El Chichón (1982), and Mt.

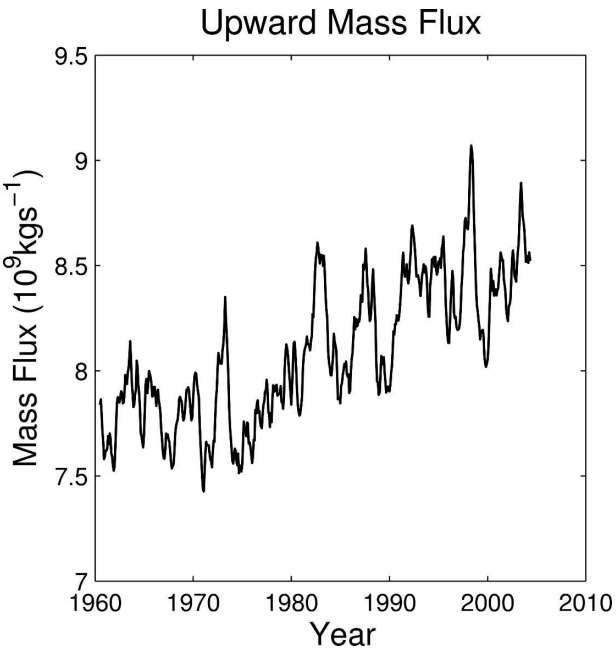

FIG. 9. The simulated upward mass flux at 77 hPa between the turnaround latitudes. Data from 1-yr running mean, averaged over all three ensemble members, are plotted.

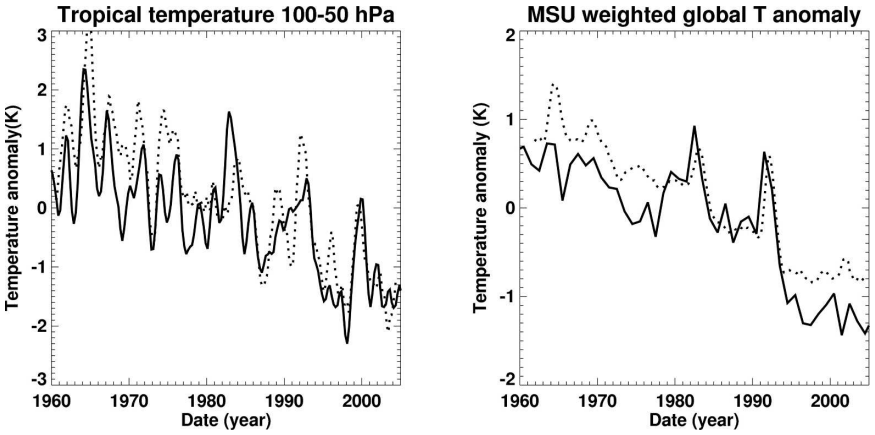

FIG. 10. Ensemble mean temperatures from the model simulations (dotted lines) compared with radiosonde data (solid lines) specified as anomalies from the 1970–99 mean (Free et al. 2005). (left) Values averaged between 20°N and 20°S, and between 100 and 50 hPa. (right) Globally averaged with MSU channel 4 vertical weighting function.

Pinatubo (1991), but there are many other short-term variations of comparable magnitude.

MSU4 is centered at about 90 hPa, representing a stable measurement of the near-tropopause temperature since the late 1970s. Radiosonde data have been compared with the MSU data, and corrections have been made to the radiosonde data to ensure consistency from 1958 onward (Free et al. 2005). Figure 10 shows the radiosonde data, although the MSU4 data were very similar during the measurement period of the latter. A 1-yr running mean has been applied to the observations and model results. The model shows overall cooling in excellent agreement with the measurements and in particular three periods of increased temperatures caused by the volcanic eruptions of Agung, El Chichón, and Mt. Pinatubo. A similar temperature analysis from observations has been shown by Parker et al. (1997), while Randel et al. (1995) showed the impact of Mt. Pinatubo on lower-stratospheric temperatures. Here, the eruptions are simulated to have a smaller temperature impact than was observed. Our results agree closely with those obtained from a suite of models (Santer et al. 2006), including the GFDL coupled ocean–atmosphere model simulation (Delworth et al. 2006; Ramaswamy et al. 2006).

Thus, both the lower-stratospheric tropical temperatures and the globally averaged MSU4-weighted temperatures show consistent features of an overall cooling, good agreement with measurements, and warming events associated with volcanic eruptions. However, Fig. 10 illustrates temperatures relative to a long-term mean. Comparison of absolute values shows that the model has a tropical tropopause cold bias of about 3–4 K. This is illustrated in a multimodel comparison including observations (Eyring et al. 2006, their Fig. 7). The results of Eyring et al. also show the model is able to reproduce the annual variation successfully, with a peak tropopause temperature in August and a minimum in about December. The impact of the temperature bias is to reduce the water saturated vapor pressure by about 40% throughout the year. This suggests that, if the saturated vapor pressure is the main influence on water vapor concentrations in the model, as indicated in observations (Randel et al. 2004; Fueglistaler and Haynes 2005), then a consistent 40% or more underprediction in stratospheric entry amount is to be expected.

b. Water vapor comparisons

Figure 11 shows the seasonal climatology of water vapor from HALOE, averaged for the period October 1991 to November 2005. The results from the model for the period 1990 to 2005 are shown in Fig. 12. Within the domain for which HALOE data are available, the qualitative agreement between the two figures is very good, albeit with a near uniform 30% low bias in the model above 100 hPa. For example, in the Tropics, the HALOE minimum value near 100 hPa, is 2.5 to 3.5 depending on season, compared with 1.5–2 ppmv in the model. In the upper stratosphere, water vapor is typically about 6–6.5 ppmv, compared with 4–4.5 ppmv in the model. The latitudinal structure of the observations is also well reproduced, with low tropical values and high values poleward of about 30°N and 30°S. The overall low bias follows from the tropical tropopause temperature bias and from the stratospheric entry concentration in Eq. (1).

Figure 13 shows the evolution of water vapor in the

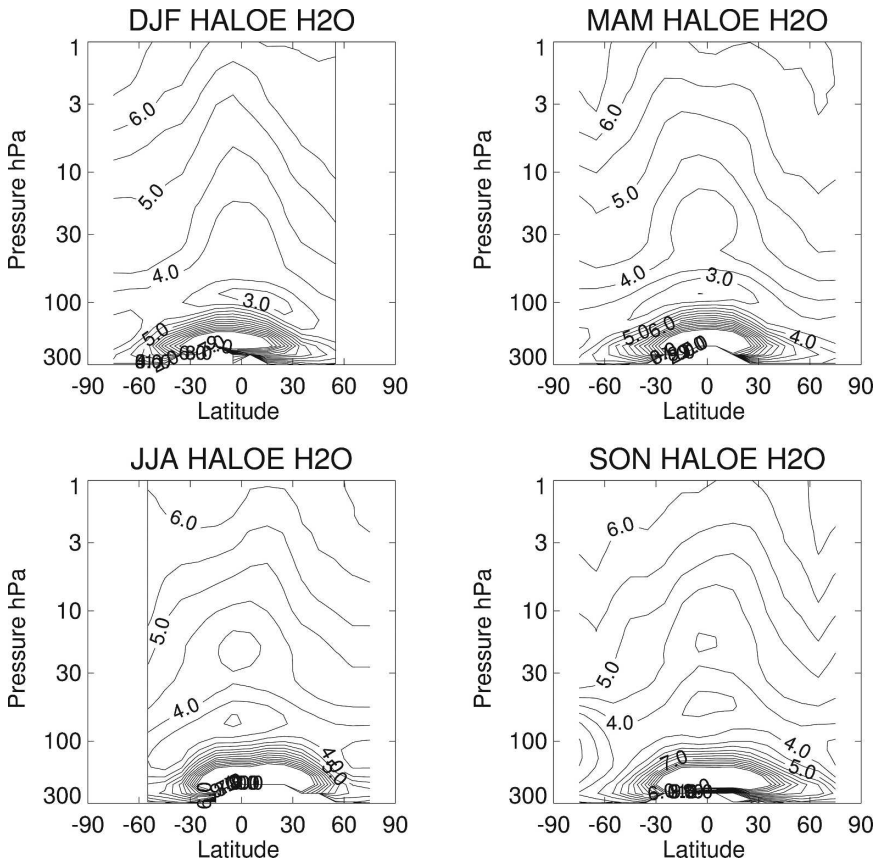

FIG. 11. Water vapor measurements from HALOE, averaged over the period October 1991 to November 2005. Observations are presented for the four seasons: December–February (DJF), March–May (MAM), June–August (JJA), and September–November (SON).

model in comparison with observations recorded from Boulder, Colorado, averaged over the pressure range from 20 to 60 hPa. The measurements [Oltmans et al. (2000) extended to the end of 2004] were taken using a frost-point hygrometer on balloon ascents averaging approximately one month apart. The data indicate a very high degree of variability compared with the signal. Also shown are data from HALOE averaged between 20 and 60 hPa for profiles that pass within 5° latitude and 20° longitude of Boulder. Model and HALOE results are also shown in the upper stratosphere. Note that the model results have all been increased by 50% for the purposes of comparison.

In the lower stratosphere, HALOE and Boulder in situ data are approximately in agreement for most of the 1990s, but diverge thereafter, as noted by Randel et al. (2004). The model has been unable to reproduce these changes quantitatively, except that since the late 1990s a significant reduction occurred. In Fig. 13, the monthly and ensemble means from the model are shown giving the (false) impression of smaller variability, but showing the daily results would make it difficult to pick out the salient features. In the upper stratosphere, a near 10% annual variation in water vapor is clearly apparent in the model simulations. The model systematic changes, after applying a 1.5 factor, also generally agree with HALOE data during the last 10 years of the simulations. This covers the period when water vapor decreased significantly in the model after the earlier slower increase from 1980 onward. Some other discrepancies are present such as the model disagreement with HALOE data in the early part of the HALOE record.

c. Discussion on water vapor changes

Water vapor amounts are notoriously difficult to measure and to simulate accurately in a coupled chemistry-climate model. However, these models are essential if all the relevant processes are to be properly considered. A fixed tropical tropopause temperature bias will provide approximately a fixed percentage error in stratospheric entry water vapor amounts, assuming that the saturated vapor pressure is the most significant physical parameter. In AMTRAC, the CH_4 concentra-

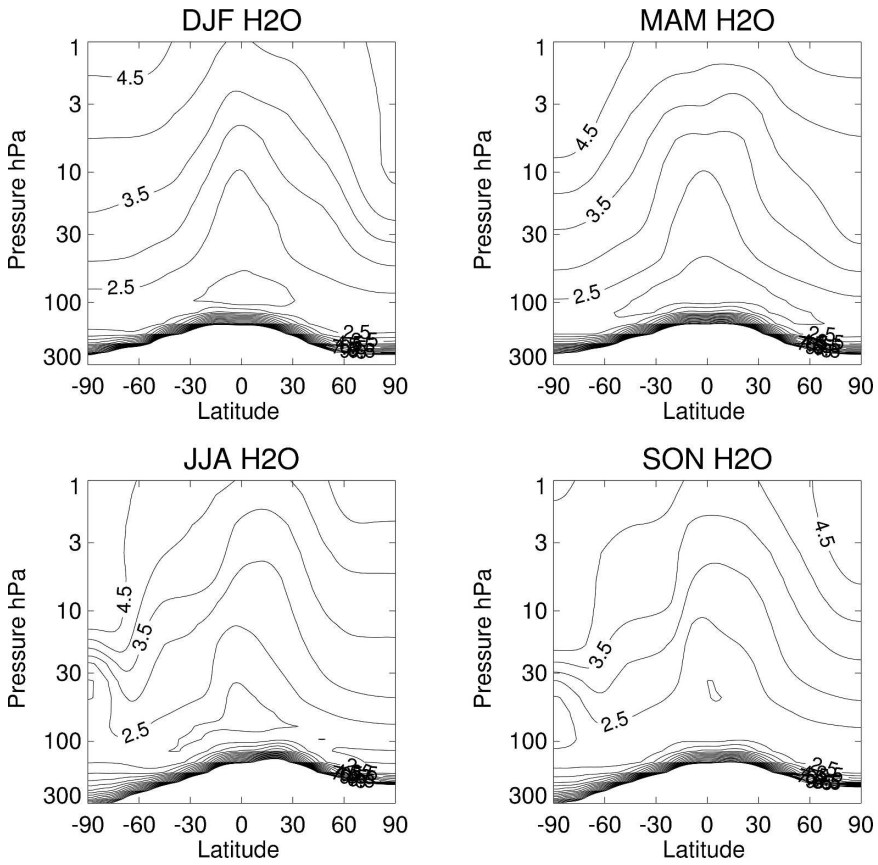

FIG. 12. Water vapor measurements from the model simulations, averaged over the period January 1990 to December 2004. Results are presented for the four seasons: DJF, MAM, JJA, and SON.

tions are also overestimated in the upper stratosphere (Eyring et al. 2006) by about 0.2 ppmv so that the methane oxidation term is smaller than in the atmosphere. The overall effect of these errors is to produce a near-uniform percentage error in simulated water vapor throughout the atmosphere. Thus, the model results obtained here are typically about 30% less than observed and, in Fig. 13a, a 50% increase in the model results was applied for comparison with observations. With that adjustment applied, some agreement with the observations over the last decade has been simulated, although many more discrepancies remain.

7. Conclusions and discussion

Episodic increases in water vapor have been demonstrated in the results of a three-member ensemble of the coupled chemistry-climate model AMTRAC. The results have shown three significant processes operating which influence water vapor amounts: water vapor amount at stratospheric entry, methane oxidation, and changes in the strength of the Brewer–Dobson circulation. Comparisons have been made with observations of the evolution of near-tropopause temperature and derived tropospheric upwelling. Apart from a systematic model cold bias, good agreement is obtained between model results and observations of the evolution of tropical temperature. This is one of the major processes driving water vapor change, since it determines the water-saturated vapor pressure in the critical cold trap entry region.

The model shows an enhanced increase in water vapor during the 1980s and 1990s followed by a decrease, qualitatively consistent with observations. The enhanced rate of increase is up to twice that expected from tropospheric methane increases alone. Agreement between model results and observations of water vapor made at Boulder, Colorado, is poor, although the decrease in the last 5–10 yr also occurs in the model. The comparisons are hampered by the infrequent sampling of the observations. Model simulations for the

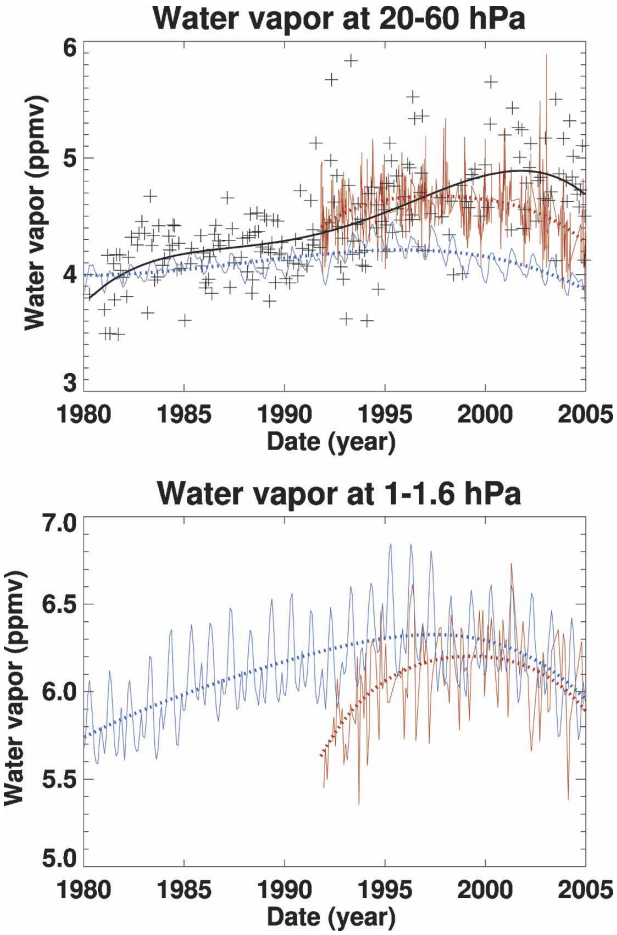

FIG. 13. (top) Comparison between model data (blue) and Boulder in situ observations (black) averaged between 20 and 60 hPa. Each individual Boulder point is plotted and each observation made over Boulder from HALOE (red) are also included. The model results are monthly means at 39.5°N, averaged over the three ensemble members. (bpttom) As in the upper panel, but for the pressure range 1 to 1.6 hPa. Since this was outside the pressure range for the Boulder data, no in situ data are included. Monthly mean HALOE data are shown for clarity. The smooth curves through each set of results are polynomial fits (order 4). Model results have been increased by 50% for the purposes of comparison.

upper stratosphere are more consistent with data from the Halogen Occultation Experiment, providing a substantial allowance is made for the model temperature and methane bias.

Volcanic eruptions have a significant impact on the tropical tropopause temperature, leading to large temperature variations observed and modeled. The model also simulated particularly rapid changes in the Brewer–Dobson circulation, as measured by the tropical upwelling (Butchart and Scaife 2001). Reductions in the age of air and increased upwelling increase the transport of methane into the stratosphere and increase substantially the water vapor concentrations via oxidation. During the rapid upwelling stage, the rate of increase of model water vapor due to methane oxidation was twice the long-term mean. Results presented here also suggest that a major volcanic eruption may affect water vapor for up to 10 yr. Evidence for this is the striking reduction in water vapor in the last 5 yr, which has been observed and modeled qualitatively, and has been shown here to be related in part to the reduction in lower-stratospheric global temperature following the eruption of Mt. Pinatubo.

The overall increase in upwelling likely occurred due to changes in the concentrations of greenhouse gases (Butchart and Scaife 2001), but the precise cause of the rapid increase in upwelling in the model results from about 1980 to the mid-1990s is difficult to diagnose in a highly coupled system. It is likely that the changes are systematic effects since they occur in each of the three ensemble members. They must therefore be driven by the external forcings, which are the sea surface temperatures (SSTs), greenhouse gases (GHGs), and chlorofluorocarbons (CFCs), and the solar cycle. The GHGs and the solar cycle may be dismissed as contributing to rapid change in upwelling, since the former changes only gradually and the latter has a near regular cycle, which would have been readily seen in the model results. While the SSTs may have contributed to the changes in upwelling, CFC changes are here favored since their concentrations contribute to substantial ozone changes. For example during the period prior to 1980, the high age of air coincided with high ozone. As the ozone amounts decreased from the late 1970s to the late 1990s the age of air decreased substantially. Further circumstantial evidence is suggested by the latitudinal dependence of the radiative impact due to observed ozone decreases, which resemble the effects due to CO_2 increase, which causes increased cooling toward the poles (Forster and Shine 1999). The implication of these pieces of evidence is that for the period of substantial ozone depletion (approximately 1980–2000) model circulation changes may be enhanced from both greenhouse gas changes (Butchart and Scaife 2001) and from ozone depletion. There are further complications in that increased water vapor in the lower stratosphere has both an increased radiative contribution affecting the circulation (Forster and Shine 1999), and increased ozone depletion via the HO_x catalytic cycle.

The results obtained here are in general agreement with previous work, most notably Fueglistaler and Haynes (2005). Our results, however, go further in suggesting that the overall water vapor changes (the anomaly of Fueglistaler and Haynes) could have occurred from possible changes in residual circulation

over the period from 1980 to 1998, which those authors did not diagnose. Indeed, given the quality of current and past meteorological measurements it has proved extremely challenging to diagnose circulation changes from analyses. A plausible hypothesis based on these model results is that the increase in the observations of water vapor over Boulder starting in about 1980 has occurred because of enhanced transport and that the recent reduction in values is merely a return to the long-term trend, driven primarily by methane oxidation and no overall transport change. Nonetheless, such a hypothesis is unable to account for the quantitative changes observed. Regarding the future, one would expect a continuing increase in the Brewer–Dobson circulation due to climate change (Butchart and Scaife 2001), tempered by ozone recovery impacts. The ozone recovery would also be expected to lead to a reduction in tropopause height and an increase in tropopause temperature, the reverse of recent history (Steinbrecht et al. 1998; Thuburn and Craig 2000). The net effect of these processes is difficult to estimate, and would be further affected by future volcanic eruptions causing temporarily enhanced water vapor.

Acknowledgments. V. Ramaswamy is thanked for his comments on this work throughout its execution and in stimulating the running of an ensemble of model simulations. Dan Schwartzkopf is thanked for supplying advice on the radiation datasets and for help with the MSU channel 4 comparison. Gera Stenchikov provided helpful advice on the volcanic aerosol datasets. G. Stenchikov, D. Schwartzkopf, and three anonymous reviewers also provided helpful comments for improving the manuscript. This work would not have been possible without the pioneering efforts of the GFDL Global Atmosphere Model Development Team. JA was funded through the University Corporation for Atmospheric Research in Boulder, Colorado. FL was funded through the Atmospheric and Oceanic Sciences Department of Princeton University.

REFERENCES

Alexander, M. J., and T. J. Dunkerton, 1999: A spectral parameterization of mean flow forcing due to breaking gravity waves. *J. Atmos. Sci.,* **56,** 4167–4182.

Anderson, J. L., and Coauthors, 2004: The new GFDL global atmosphere and land model AM2/LM2: Evaluation with prescribed SST simulations. *J. Climate,* **17,** 4641–4673.

Andrews, A. E., and Coauthors, 2001: Mean ages of stratospheric air derived from in situ observations of CO_2, CH_4, and N_2O. *J. Geophys. Res.,* **106,** 32 295–32 314.

Austin, J., and N. Butchart, 2003: Coupled chemistry-climate model simulations for the period 1980 to 2020: Ozone depletion and the start of ozone recovery. *Quart. J. Roy. Meteor. Soc.,* **129,** 3225–3249.

——, and F. Li, 2006: On the relationship between the strength of the Brewer-Dobson circulation and the age of stratospheric air. *Geophys. Res. Lett.,* **33,** L17807, doi:10.1029/2006GL026867.

——, and R. J. Wilson, 2006: Ensemble simulations of the decline and recovery of stratospheric ozone. *J. Geophys. Res.,* **111,** D16314, doi:10.1029/2005JD006907.

——, and Coauthors, 2003: Uncertainties and assessments of chemistry-climate models of the stratosphere. *Atmos. Chem. Phys.,* **3,** 1–27.

Boering, K. A., S. C. Wofsy, B. C. Daube, H. R. Schneider, M. Loewenstein, and J. R. Podolske, 1996: Stratospheric mean ages derived from observations of CO_2 and N_2O. *Science,* **274,** 1340–1343.

Butchart, N., and A. A. Scaife, 2001: Removal of chlorofluorocarbons by increased mass exchange between the stratosphere and the troposphere in a changing climate. *Nature,* **410,** 799–802.

——, and Coauthors, 2006: A multi-model study of climate change in the Brewer-Dobson circulation. *Climate Dyn.,* **27,** 727–741.

Christy, J. R., R. W. Spencer, and W. D. Braswell, 2000: MSU tropospheric temperatures: Dataset construction and radiosonde comparisons. *J. Atmos. Oceanic Technol.,* **17,** 1153–1170.

Dameris, M., and Coauthors, 2005: Long-term changes and variability in a transient simulation with a chemistry-climate model employing realistic forcing. *Atmos. Chem. Phys. Discuss.,* **5,** 2297–2353.

Delworth, T. L., and Coauthors, 2006: GFDL's CM2 global coupled climate models. Part I: Formulation and simulation characteristics. *J. Climate,* **19,** 643–674.

Eyring, V., and Coauthors, 2006: Assessment of temperature, trace species, and ozone in chemistry-climate model simulations of the recent past. *J. Geophys. Res.,* **111,** D22308, doi:10.1029/2006JD007327.

Forster, P. M. D., and K. P. Shine, 1999: Stratospheric water vapour changes as a possible contributor to observed stratospheric cooling. *Geophys. Res. Lett.,* **26,** 3309–3312.

Free, M., D. J. Seidel, J. K. Angell, J. Lanzante, I. Durre, and T. C. Peterson, 2005: Radiosonde atmospheric temperature products for assessing climate (RAT-PAC): A new data set of large-area anomaly time series. *J. Geophys. Res.,* **110,** D22101, doi:10.1029/2005JD006169.

Fueglistaler, S., and P. H. Haynes, 2005: Control of interannual and longer term variability of stratospheric water vapor. *J. Geophys. Res.,* **110,** D24108, doi:10.1029/2005JD006019.

Hall, T. M., D. W. Waugh, K. A. Boering, and R. A. Plumb, 1999: Evaluation of transport in stratospheric models. *J. Geophys. Res.,* **104,** 18 815–18 839.

Harries, J. E., and Coauthors, 1996: Validation of measurements of water vapor from the Halogen Occultation Experiment, HALOE. *J. Geophys. Res.,* **101,** 10 205–10 216.

Hartmann, D. L., J. R. Holton, and Q. Fu, 2001: The heat balance of the tropical tropopause, cirrus, and atmospheric dehydration. *Geophys. Res. Lett.,* **28,** 1969–1972.

Holton, J. R., and A. Gettelman, 2001: Horizontal transport and the dehydration of the stratosphere. *Geophys. Res. Lett.,* **28,** 2799–2802.

Jones, R. L., and J. A. Pyle, 1984: Observations of CH_4 and N_2O by the Nimbus 7 SAMS: A comparison of in situ data and

two-dimensional numerical model calculations. *J. Geophys. Res.,* **89,** 5263–5279.

Joshi, M. M., and K. P. Shine, 2003: A GCM study of volcanic eruptions as a cause of increased stratospheric water vapor. *J. Climate,* **16,** 3525–3534.

Lean, J., J. Beer, and R. S. Bradley, 1995: Reconstruction of solar irradiance since 1610: Implications for climate change. *Geophys. Res. Lett.,* **22,** 3195–3198.

Le Texier, H., S. Solomon, and R. R. Garcia, 1988: The role of molecular hydrogen and methane oxidation in the water vapour budget of the stratosphere. *Quart. J. Roy. Meteor. Soc.,* **114,** 281–295.

Lin, S.-J., 2004: A "vertically Lagrangian" finite volume dynamical core for global models. *Mon. Wea. Rev.,* **132,** 2293–2307.

Oltmans, S. J., H. Vömel, D. J. Hofmann, K. Rosenlof, and D. Kley, 2000: The increase in stratospheric water vapor from balloon borne frostpoint hygrometer measurements at Washington, D.C. and Boulder, Colorado. *Geophys. Res. Lett.,* **27,** 3453–3456.

Park, J. H., M. K. W. Ko, C. H. Jackman, R. A. Plumb, J. A. Kaye, and K. H. Sage, 1999: Models and measurements intercomparison II. Tech. Memo. NASA/TM-1999-209554, 502 pp.

Parker, D. E., M. Gordon, D. P. N. Cullum, D. M. H. Sexton, C. K. Folland, and N. Rayner, 1997: A new global gridded radiosonde temperature data base and recent temperature trends. *Geophys. Res. Lett.,* **24,** 1499–1502.

Ramaswamy, V., M. D. Schwarzkopf, W. J. Randel, B. D. Santer, B. J. Soden, and G. L. Stenchikov, 2006: Anthropogenic and natural influences in the evolution of lower stratospheric cooling. *Science,* **311,** 1138–1141.

Randel, W. J., F. Wu, J. M. Russell III, J. W. Waters, and L. Froidevaux, 1995: Ozone and temperature changes in the stratosphere following the eruption of Mount Pinatubo. *J. Geophys. Res.,* **100,** 16 753–16 764.

——, ——, S. J. Oltmans, K. Rosenlof, and G. E. Nedoluha, 2004: Interannual changes of stratospheric water vapor and correlations with tropical tropopause temperatures. *J. Atmos. Sci.,* **61,** 2133–2148.

Remsberg, E. E., J. M. Russell III, L. L. Gordley, J. C. Gille, and P. L. Bailey, 1984: Implications of stratospheric water vapor distribution as determined from the Nimbus 7 LIMS experiment. *J. Atmos. Sci.,* **41,** 2934–2945.

Rood, R. B., 2005: Assimilation of stratospheric meteorological and constituent observations: A review. *SPARC Newsletter,* No. 25, 31–37.

Rosenlof, K. H., and Coauthors, 2001: Stratospheric water vapor increases over the past half-century. *Geophys. Res. Lett.,* **28,** 1195–1198.

Russell, J. M., III, A. F. Tuck, L. L. Gordley, J. H. Park, S. R. Drayson, J. E. Harries, R. J. Cicerone, and P. J. Crutzen, 1993: The Halogen Occultation Experiment. *J. Geophys. Res.,* **98,** 10 777–10 797.

Sander, S. P., and Coauthors, 2003: Chemical kinetics and photochemical data for use in atmospheric studies. Tech. Rep. evaluation number 14, JPL Publication 02-25, 334 pp.

Santer, B. D., J. E. Penner, and P. W. Thorne, 2006: How well can the observed vertical temperature changes be reconciled with our understanding of the causes of these changes? Temperature Trends in the Lower Atmosphere: Steps for Understanding and Reconciling Differences. T. R. Karl et al., Eds., Tech. Rep., U.S. Climate Change Science Program and the Subcommittee on Global Change Research, NOAA, NCDC, x+164 pp.

Sato, M., J. E. Hansen, M. P. McCormick, and J. B. Pollack, 1993: Stratospheric aerosol optical depths, 1850–1990. *J. Geophys. Res.,* **98,** 22 987–22 994.

Schoeberl, M., A. R. Douglass, B. Polansky, C. Boone, K. A. Walker, and P. Bernath, 2005: Estimation of stratospheric age spectrum from chemical tracers. *J. Geophys. Res.,* **110,** D21303, doi:10.1029/2005JD006125.

Seidel, D., R. J. Ross, J. K. Angel, and G. C. Reid, 2001: Climatological characteristics of the tropical tropopause as revealed by radiosondes. *J. Geophys. Res.,* **106,** 7857–7878.

Steinbrecht, W., H. Claude, U. Köhler, and K. P. Hoinka, 1998: Correlations between tropopause height and total ozone: Implications for long-term changes. *J. Geophys. Res.,* **103,** 19 183–19 192.

Stenchikov, G. L., I. Kirchner, A. Robock, H.-F. Graf, J. C. Antuña, R. G. Grainger, A. Lambert, and L. Thomason, 1998: Radiative forcing from the 1991 Mount Pinatubo volcanic eruption. *J. Geophys. Res.,* **103,** 13 837–13 857.

Thomason, L. W., and L. R. Poole, 1997: A global climatology of stratospheric aerosol surface area density deduced from Stratospheric Aerosol and Gas Experiment II measurements: 1984–1994. *J. Geophys. Res.,* **102,** 8967–8976.

Thuburn, J., and X. Craig, 2000: Stratospheric influence on tropopause height: The radiative constraint. *J. Atmos. Sci.,* **57,** 17–28.

Waugh, D. W., and T. M. Hall, 2002: Age of stratospheric air: Theory, observations and models. *Rev. Geophys.,* **40,** 1010, doi:10.1029/2000RG000101.